UDC 620.181; 542.9 https://doi.org/10.33619/2414-2948/63/18

THE TRANSITION METAL AND NON-METAL CO-DOPING GRAPHENE FOR OXYGEN REDUCTION REACTION ELECTROCATALYSIS: A DENSITY FUNCTIONAL THEORY STUDY

©Chen Fengxiang, *ORCID: 0000-0002-2229-0884, Ogarev Mordovia State University; Jiangsu University of Science and Technology, Saransk, Russia Zhenjiang, China, chenfengxiangjinan@163.com*
©Yang Lei, *Jiangsu University of Science and Technology, Zhenjiang, China, yljust18@163.com*

ПЕРЕХОДНЫЙ МЕТАЛЛ И НЕМЕТАЛЛИЧЕСКИЙ СО-ЛЕГИРУЮЩИЙ ГРАФЕН ДЛЯ ЭЛЕКТРОКАТАЛИЗА РЕАКЦИИ ВОССТАНОВЛЕНИЯ КИСЛОРОДА: ИССЛЕДОВАНИЕ ФУНКЦИОНАЛЬНОЙ ТЕОРИИ ПЛОТНОСТИ

©Чэнь Фэнсян, *ORCID: 0000-0002-2229-0884, Национальный исследовательский Мордовский государственный университет им. Н. П. Огарева; Цзянсуский университет науки и техники, г. Саранск, Россия; г. Чжэньцзян, Китай, chenfengxiangjinan@163.com*
©Ян Лэй, *Цзянсуский университет науки и техники, г. Чжэньцзян, Китай, yljust18@163.com*

Abstract. Proton exchange membrane fuel cells (PEMFCs) are vital energy-conversion devices in a hydrogen-fueled economic. In this study, we performed density functional theory (DFT) calculations to study $4e^-$ oxygen reduction reaction process on transition metal embedded in single and double vacancies (SV and DV) in a graphene. We calculated bonding energy and adsorption energy on CoX_3 (X = B, C, N, Si, P and S) and CoX_4 (X = B, C, N, Si, P and S) embedded in graphene. Our DFT results indicate that formation of CoX_3 is unfeasible and the formation of CoX_4 is feasible. In addition, the crucial role of ligand atoms near embedded metal atoms is revealed via the molecular orbital theory. Then the Gibbs free energy of CoX_4 are calculated and the CoN_4, CoS_4, and CoP_4 are predicted to be active for catalyzing ORR, and these also show ligand atoms' coordination effect for catalytic activity of central metal. Furthermore, we observed that they have identical rate-determining step (RDS). This work can provide some references for transition atoms catalytic doped in carbon materials.

Аннотация. Топливные элементы с протонообменной мембраной (PEMFCs) являются жизненно важными устройствами для преобразования энергии в водородной экономике. В этом исследовании мы выполнили расчеты теории функционала плотности (DFT) для изучения процесса реакции восстановления $4e^-$ кислорода на переходном металле, внедренном в одиночные и двойные вакансии (SV и DV) в графене. Мы рассчитали энергию связи и энергию адсорбции для CoX_3 (X = B, C, N, Si, P и S) и CoX_4 ((X = B, C, N, Si, P и S), внедренных в графен. Наши результаты DFT показывают, что образование CoX_3 невозможно, а образование CoX_4 возможно. Кроме того, решающая роль атомов лиганда вблизи внедренных атомов металла раскрывается с помощью теории молекулярных орбиталей. Затем рассчитывается свободная энергия Гиббса CoX_4, и предполагается, что CoN_4, CoS_4 и CoP_4 будут активными для катализирования ORR, и они также демонстрируют эффект координации атомов лиганда для каталитической активности центрального металла. Кроме

Т. 7. №2. 2021
https://doi.org/10.33619/2414-2948/63

того, мы заметили, что у них идентичный шаг определения скорости (RDS). Эта работа может предоставить некоторые ссылки на переходные атомы, каталитически легированные в углеродных материалах.

Keywords: PEMFCs, oxygen reduction reaction, density functional theory, coordination effect.

Ключевые слова: PEMFCs, реакция восстановления кислорода, теория функционала плотности, координационный эффект.

Research Background and Theoretical Research

The concerns over the hasty depletion of fossil fuels, the cumulative increase in energy consumption and the associated ecological issues have compelled society to explore the polymer electrolyte membrane fuel cell (PEMFC) for the future energy utilization. The further commercialization of such promising technology is seriously hindered by the state-of-the-art electrocatalysts Pt for the oxygen reduction reaction (ORR) with the operation voltages are 0.8 V, being away from the theoretical 1.23 V and then accounting for the energy consumption [1]. Furthermore, the high cost and the natural scarcity of the noble metal hamper its economical attraction. In the regard, it is clear challenging but indispensable to design the earth-abundant alternatives with superior electrochemical performance to boost the reaction and minimize the usage of the noble metals.

Inspired by the pioneering work portraying the impressive ORR activity of macrocycles containing transition metal (TM) coordinated with the nitrogen in 1964, the development of the graphene with TM/N motifs is vigorous due to the advantages of the adjustable performance and atomic utilization [2]. Generally, since the catalytic ability is directly related with the TM *d* orbital level according to the famous *d* band model [3], selecting the TM element with suitable *d* band center is a common strategy to overcome the ORR sluggish kinetics [4]. Herein, the active sites consisted by FeN_4 or CoN_4 are identified by both theoretical and experimental investigations. In addition, based on the ligand-field effects, the variability in *d* orbital of the TM atom could be achieved by altering the coordinated elements with dissimilar electronic structures as well as the different concentration [5]. Such strategy is confirmed by the presence of Fe/S, Fe/P or Co/P embedded graphene with the superior electrocatalytic performance beyond the TM/N combination [6]. Furthermore, our recent work focused on the TM/O co-doping graphene reveals the high efficiency of the NiO_2C_2 configuration acted as the oxygen electrode materials, further supporting the tailoring effect of the coordination environment on the TM reactivity [7]. Indeed, the interaction between the TM and its local coordinated environment provides the so-called synergetic effect. However, the unambiguous investigation on the physical origination at the atomic level is untouched. In the regard, in order to the targeted design, it is imperative to get in-depth insight into the influence of the interactions between the TM and local environment on the corresponding electrocatalysis.

In this manuscript, density functional theory (DFT) calculations are used within an electrochemical framework to analyze the ORR electrocatalysis. Herein, the CoX_n embedded graphene (X = B, C, N, Si, P, S; n = 3, 4) are systematically studied, as schematically shown in Figure 1. Our goal is located at the influence of the local environment, the Co selection as the reprehensive TM element is reasonable due to the high activity [8–9]. Both metal center and ligand atoms are considered as adsorption site for oxygen atom. the adsorption behavior of

Т. 7. №2. 2021
https://doi.org/10.33619/2414-2948/63

the intermediates is preferentially calculated, which allows valuating the scaling relationship and thermodynamic free energy. Via analyzing partial density of states (PDOS) and the Mulliken charge, the relationship between the activity and the electronic structures is revealed. The data provide the fundamental understanding of the variation of the TM reactivity caused by the local environment and further identify the optimal candidate to guide the top-down experimental syntheses.

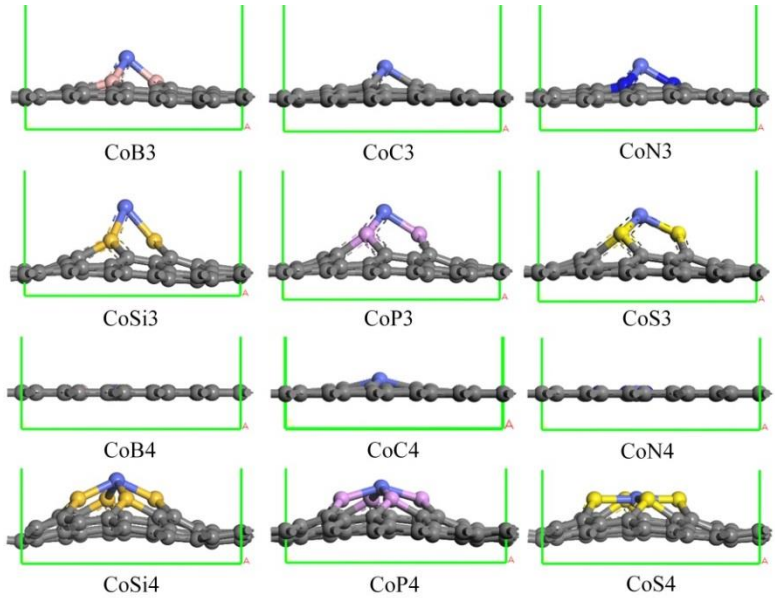

Figure 1. The optimized structures of CoX_n embedded graphene.

Computation method

All calculations are performed within the DFT framework as implemented in $DMol^3$ code [10–11]. The generalized gradient approximation with the Perdew–Burke–Ernzerhof (PBE) functional is employed to describe exchange and correlation effects [12]. The DFT Semi-core Pseudopots (DSPP) core treat method is implemented for relativistic effects, which replaces core electrons by a single effective potential and introduces some degree of relativistic correction into the core [13]. The double numerical atomic orbital augmented by a polarization function (DNP) is chosen as the basis set [10]. A smearing of 0.005 Ha (1 Ha = 27.21 eV) to the orbital occupation is applied to achieve accurate electronic convergence. In order to ensure high-quality results, the real-space global orbital cutoff radius is set as high as 5.2 Å. In the geometry structural optimization, the convergence tolerances of energy, maximum force and displacement are 1.0×10^{-5} Ha, 0.002 Ha/Å and 0.005 Å, respectively. The spin-unrestricted method is used for all calculations. A conductor-like screening model (COSMO) was used to simulate a H_2O solvent environment for all calculations [14]. COSMO is a continuum model in which the solute molecule forms a cavity within the dielectric continuum. The $DMol^3$/COSMO method has been generalized to periodic boundary cases. The dielectric constant is set as 78.54 for H_2O. Some previous results have shown that this implicit solvation model is an effective method to describe solvation [15–16]. The 15 Å-thick vacuum is added to avoid the artificial interactions between the functional graphene monolayer and its images.

It is generally believed that the ORR of a fuel cell has two reaction mechanisms: one is that O_2 is directly reduced to H_2O ($O_2 + 4H^+ + 4e^- \rightarrow 2H_2O$), called the four-electron process; the other is O_2 to form the metastable H_2O_2 ($O_2 + 2H^+ + 2e^- \rightarrow H_2O_2$), called the two-electron process. The

Т. 7. №2. 2021
https://doi.org/10.33619/2414-2948/63

difference is whether the hydrogen peroxide is produced before the O–O bond breaks. Previous experiments show that [17], the four-electron process is the main process, and the efficiency is much higher than that of the two-electron process. Therefore, we only discuss the four-electron process. In order to evaluate the performance of ORR electrocatalyst, we consider the four-electron association mechanism as the possible reaction path of the cathode:

$$O_2(g)+ * + (H++ e^-) \rightarrow OOH^* \text{ (R1)}$$
$$OOH^*+ (H^++ e^-) \rightarrow O^* + H_2O(l) \text{ (R2)}$$
$$O^* + (H^++ e^-) \rightarrow OH^* + H_2O(l) \text{ (R3)}$$
$$OH^* + (H^++ e^-) \rightarrow 2H_2O(l) \text{ (R4)}$$

Where the asterisk (*) represents an active site on the catalyst surface, (l) and (g) refer to liquid phase and gas phase, respectively.

In the reaction energy landscape, all ORR intermediates are described as proton/electron ($H^+ + e^-$) transfers [18]. The adsorption energy of the corresponding intermediates are calculated by the following,

$$E_{ads}(M) = E_{sys} - E_{substrate} - E_M \quad (1)$$

where E_{sys}, $E_{substrate}$ and E_M are the total energy of the adsorption systems, the functional graphene and ORR intermediate, respectively. $E_{ads} < 0$ corresponds to an exothermic adsorption process.

The Gibbs free energy changes (ΔG) of the ORR elemental steps have been calculated according to the computational hydrogen electrode (CHE) model developed by Nørskov et. al. where the chemical potential of proton/electron ($H^+ + e^-$) in solution is equal to the half of the chemical potential of a gas-phase H_2. The ΔG for every elemental step can be determined as following:

$$\Delta G = \Delta E + \Delta ZPE - T\Delta S + \Delta G_{pH} + \Delta G_U \quad (2)$$

where ΔE is the electronic energy difference based on DFT calculations, ΔZPE implies the change in zero-point energy, T denotes the temperature (equal to 298.15 K here), ΔS shows the change in the entropy, and ΔG_{pH} and ΔG_U are the free energy contributions due to variation in pH values (pH is set as 0 in acid medium and 14 in alkaline medium) and electrode potential U, respectively. The zero-point energies and entropies of the ORR intermediates are calculated from the vibrational frequencies according to standard methods. Following the suggestion of Wilcox, et. al. [19], in order to reduce the calculation, the monolayer is fully constrained. $\Delta G < 0$ corresponds to an exothermic adsorption process. The free energy G of O_2 is derived as $G(O_2) = 4.92+2G(H_2O)–2G(H_2)$ by utilizing OER equilibrium at the standard conditions 12.

Results

Figure 1 presents the optimized structures of CoX_n embedded graphene. Severe deformation of the graphene is induced by the inserting the CoP_n, $CoSi_n$ and CoS_n motifs whilst the flatness is preserved for the CoB_n, CoC_n and CoN_n, respectively, in consistence with the previous results. In order to uncover the ligand influence on the Co electronic structure, the partial density of states (PDOS) of CoP_n are analyzed as the representative. As shown in Figure 2, the clear overlaps of the *pd* band are observed where the Co d-orbital is concentrated above −5 eV and the P *p*-orbital is ranged from −10 to 5 eV, indicating the strong *pd* orbital hybridization. Therein, besides the Fermi energy, the hybridized peaks are distinguished at −0.77, −1.84 and −4.55 eV for CoP_3 and −1.76, −2.58 and −4.24 eV for CoP_4, respectively. Furthermore, the P *s*-electron distribution is mainly

Т. 7. №2. 2021
https://doi.org/10.33619/2414-2948/63

varied from −15 to −10 eV, revealing the faint effect on the Co *d*-band. Due to the PDOS similarity, it is concluded that the binding between Co and its environment is originated from the *pd* interaction. Herein, the corresponding Co *d*-band center ε_d is summarized in Table 1.

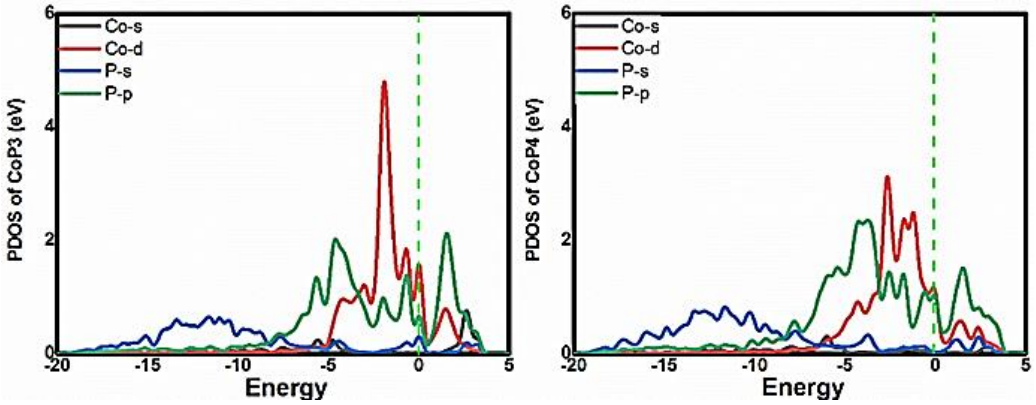

Figure 2. The partial density of states (PDOS) of CoP_n.

Table 1.

THE GEOMETRIC AND ELECTRONIC STRUCTURES OF THE CoX_n EMBEDDED GRAPHENE

	CoB_4	CoC_4	CoN_4	$CoSi_4$	CoP_4	CoS_4	CoB_3	CoC_3	CoN_3	$CoSi_3$	CoP_3	CoS_3
$d_{Co\text{-}X}$	1.89	1.92	1.89	2.14	2.08	2.13	1.87	1.78	1.85	2.19	2.03	2.05
$h_{Co\text{-}G}$	0.00	0.03	0.00	0.13	0.10	0.08	0.10	0.08	0.08	0.16	0.15	0.14
E_b	−3.28	−6.52	−7.91	−6.29	−6.18	−3.84	−3.39	−7.97	−4.79	−4.41	−4.54	−2.73
ε_d	−2.71	−1.59	−1.85	−2.00	−2.77	−1.23	−1.15	−2.36	−1.49	−1.44	−1.95	−1.85
M_{Co}	−0.55	−0.29	0.13	−0.87	−0.92	−0.51	−0.32	−0.20	0.23	−0.34	−0.59	−0.29
M_X	0.22	−0.05	−0.42	0.81	0.64	−0.00	0.26	0.02	−0.41	0.73	0.61	0.02

In order to character the sufficiency of the O_2 activation, the important step of O_2 adsorption molecule on CoX_n embedded graphene is examined. Due to similarity, the CoP_3 and CoP_4 are acted as the representatives. The corresponding adsorption energies are listed in Table 1. The O_2 molecule prefers to chemically suit at the Co atom via the end-on configuration where the corresponding length of Co–O bond and O–O bond are 1.693 Å and 1.295 Å for CoP_3, 1.864 Å and 1.305 Å for CoP_4, respectively. According to the Mulliken charge analysis, charge is transferred from the substrate to the adsorbed O_2 molecule. Furthermore, the partial density of states clearly reveals the obvious hybridization between the O_2 p-orbital and the Co *d*-orbital of CoP_4 in Figure 3, besides the Fermi energy, the hybridized peaks is at −2.50, being accounted for the O_2 activation, which correlates with the elongation of the O–O bond.

We use graphene as the catalytic substrate and transition metal Co is doped on the single and double vacancies. Such a structure can be associated with a substitutional impurity in graphene. The transition metal has a larger atomic radius than the carbon atom. In the single vacancy substitution doping, the Co atom will protrude from the surface of the graphene, as shown in Figure 1, which is about 1.3 Å above the surface, and correspondingly the height is much smaller protruded in the double vacancy, which is in same ligand element-nitrogen. Due to the different nature of the ligand atoms, CoX4 structure will show different structures, such as non-metallic elements such as P, S, Si, etc. Atomic radius and electronegativity are far different from carbon atoms, which will result in ligand atoms, even with the protrusion of surrounding carbon atoms, the structural stability is reduced to varying degrees.

Т. 7. №2. 2021
https://doi.org/10.33619/2414-2948/63

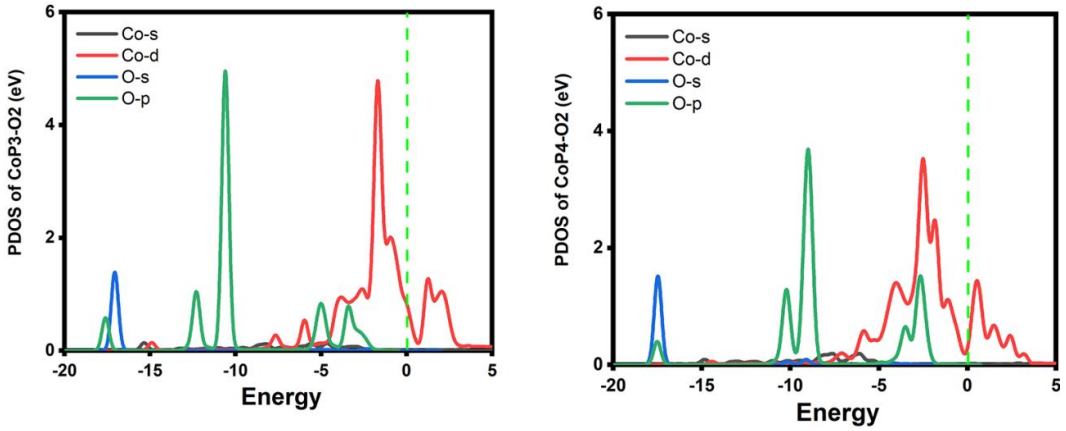

Figure 3. The PDOS of O_2 adsorbed CoP_n.

In the cathodic electrocatalytic reaction, the surface of the carbon-based catalyst acts as reaction sites, and the adsorption and desorption of O_2 and several oxygen-containing intermediates requires moderate strength and conforms to the volcanic principle, so that the reaction can be carried out quickly and stably. At the same time, the catalyst requires high stability. As shown in Table 1, we calculate the stability of all structure forms, we can see that the binding energy of CoN_4 is −7.91 eV, which has good stability.

According to the four-electron association mechanism in (R1), (R2), (R3), (R4), we calculated the catalytic properties of three ORR intermediates O, OH, OOH. The advantageous adsorption properties of ORR intermediates are prerequisites for the reaction to proceed. The results of adsorption energies are shown in Table 2. It can be seen that adsorption energies of CoX_4 to OOH ranges from −1.48 to −3.76 eV, and that of O is from −2.98 to −5.99 eV, and adsorption energies of OH values ranged from −2.65 to −5.05 eV, of which CoB_4 has the strongest adsorption energy for three intermediates. In addition to B ligand doping, adsorption energies of CoX_3 are stronger than that of CoX_4. According to the previous reaction formulas (R1)(R2)(R3)(R4), the front two reactions are mainly adsorption of OOH and O–O bond cleavage in ORR, and the latter two reactions mainly involve the formation and desorption of H_2O molecules. CoB_4 and CoX_3 have strong adsorption capacity, but they are not conducive to the desorption of H_2O. CoN_4, CoS_4, and CoP_4 can be considered as oxygen reduction electrocatalysts.

Table 2.

THE ADSORPTION OF REACTANT O_2 AND THE ORR INTERMEDIATES (eV)

	CoB_4	CoC_4	CoN_4	$CoSi_4$	CoP_4	CoS_4	CoB_3	CoC_3	CoN_3	$CoSi_3$	CoP_3	CoS_3
$E_{ads}(O_2)$	−3.33	−1.30	−0.73	−1.56	−0.66	−0.58	−1.62	−1.40	−3.10	−1.98	−1.95	−2.05
E_{ads}(OOH)	−3.76	−1.96	−1.76	−2.13	−1.53	−1.48	−2.47	−2.78	−3.05	−2.88	−2.22	−2.32
E_{ads}(O)	−5.99	−4.17	−3.11	−4.43	−3.13	−2.98	−4.29	−4.60	−5.76	−5.6	−4.87	−4.59
E_{ads}(OH)	−5.05	−3.12	−2.84	−3.43	−2.65	−2.67	−3.72	−4.03	−4.33	−4.17	−3.71	−3.55
$E_{ads}(O_2)$-side	−3.33	−1.30	−0.73	−1.56	−0.66	−0.56	−1.61	−1.40	−3.05	−1.98	−1.95	−2.05
$E_{ads}(O_2)$-end	−2.66	−1.14	−0.73	−1.20	−0.55	−0.58	−1.62	−1.38	−3.10	−1.98	−1.63	−1.65
d_{O-O}	1.39	1.40	1.31	1.38	1.31	1.33	1.39	1.39	1.45	1.42	1.42	1.40
M_{O2}	−0.52	−0.45	−0.40	−0.52	−0.39	−0.48	−0.50	−0.54	−0.73	−0.59	−0.63	−0.58

Based on the data in Table 2, E(O), E(OH), and E(OOH) were used as a function of adsorption energy of OH, and a dot plot was drawn and fitted, as shown in Figure 4. We can get the

Т. 7. №2. 2021
https://doi.org/10.33619/2414-2948/63

linear relationship of ORR intermediates about E(OH):

$$E_{ads}(OOH)=0.93E_{ads}(OH)+3.05 \quad (4)$$

$$E_{ads}(O)=1.46E_{ads}(OH)+1.92 \quad (5)$$

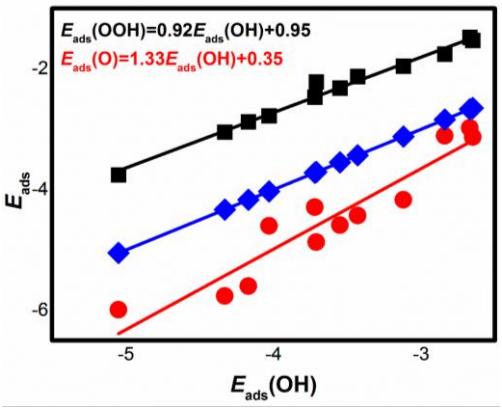

Figure 4 The adsorption energy E_{ads} of the ORR intermediates as a function of E_{ads}(OH).

The fitted line slope is comparable to that of porphyrins, and the adsorption energy of O is not much discrete with respect to E(OH). According to the data in Table 2, it can be seen that different ligand atoms have a certain regulation effect on the ORR catalytic performance of metal centers. The E_{ads} data of N, S and P doping differs little, and the catalytic performance. It is known from previous studies that in the transition metal doping, the carbon atoms bonded to the metal center may be oxidized, leading the central metal to electrons, prolonging the C–M bond, and strengthening the bonding of the O-M bond. When other carbon atoms are oxidized, it may cause weakening of the active center. On the contrary, N, P, etc. are hardly oxidized due to their electronegativity, ensuring a stable framework of the catalyst.

Table 3.

THE GIBBS FREE ENERGY *G* AT THE POTENTIAL OF 0V AND 1.23 V

		CoB_4	CoC_4	CoN_4	$CoSi_4$	CoP_4	CoS_4	CoB_3	CoC_3	CoN_3	$CoSi_3$	CoP_3	CoS_3
	OOH	1.10	3.11	3.38	3.43	3.39	3.51	2.50	2.29	1.91	2.11	2.83	2.66
$U = 0$	O	−0.65	1.38	2.44	0.98	2.32	2.47	1.12	0.88	−0.14	−0.05	0.70	0.90
	OH	−1.87	0.15	0.56	−0.14	0.58	0.61	−0.45	−0.74	−0.99	−0.88	−0.39	−0.25
	OOH	−2.59	−0.58	−0.31	−0.26	−0.30	−0.18	−1.19	−1.40	−1.78	−1.58	−0.86	−1.03
$U = 1.23$	O	−3.11	−1.08	−0.02	−1.48	−0.14	0.01	−1.34	−1.58	−2.60	−2.51	−1.76	−1.56
	OH	−3.10	−1.08	−0.67	−1.37	−0.65	−0.62	−1.68	−1.97	−2.22	−2.11	−1.62	−1.48

It can be seen from the foregoing that the double vacancy doping has better performance than the single vacancy, and we calculated the free energy of the double vacancies doping with reaction intermediates as shown in Table 3. It can be seen from Fig. 5 that when the potential is 0 V, apart from CoB_4 and $CoSi_4$, all catalytic materials are exothermic reaction steps. The formation step of H_2O is the slowest step in each catalytic structures, and when the potential is 1.23V, there is an energy barrier in the O–O bond splitting step and the H_2O forming step, and the R4 step is most notable, which reaches around 0.65 eV, it is the thermodynamic rate-determining step (RDS) in all steps. In summary, it can be determined that R4 is RDS of the reaction, the minimum is about 0.6 eV at 1.23 V, which is expressed as being difficult to desorb in the reaction. Among them, CoN_4, CoP_4 and CoS_4 have better performance, which is consistent with the previous analysis.

Т. 7. №2. 2021
https://doi.org/10.33619/2414-2948/63

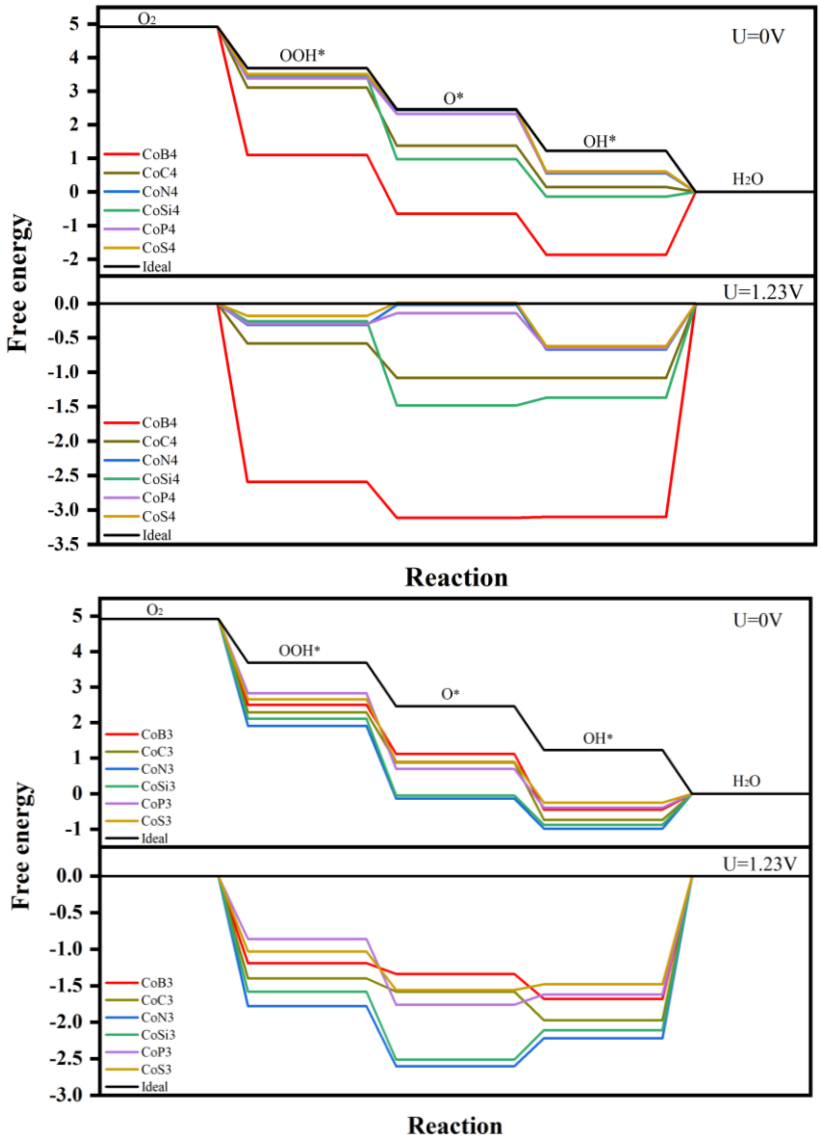

Figure 5. The Gibbs free energy G (a).

Conclusion

According to the first principal calculation, the catalytic performance of transition metal and different ligand atoms embedded graphene in the oxygen reduction reaction was studied. The adsorption energy of O and OOH has a linear relationship with the OH adsorption energy, it shows the adjustment of the catalytic properties of the central metal by ligand atoms. CoN_4, CoS_4 and CoP_4 have better performance than other catalytic structures. They have the same rate determining step in the desorption process. The adsorption energy of OH is about 0.4 eV higher than that of Pt (The adsorption energy of the surface of Pt(1 1 1) is −2.26 eV), resulting in higher energy barriers. In all aspects, CoN_4, CoS_4 and CoP_4 have similar properties and enhanced catalysis activity.

References:

1. Nørskov, J. K., Rossmeisl, J., Logadottir, A., Lindqvist, L. R. K. J., Kitchin, J. R., Bligaard, T., & Jonsson, H. (2004). Origin of the overpotential for oxygen reduction at a fuel-cell cathode. *The Journal of Physical Chemistry B*, *108*(46), 17886-17892. https://doi.org/10.1021/jp047349j

2. Chen, Z. W., Chen, L. X., Yang, C. C., & Jiang, Q. (2019). Atomic (single, double, and triple atoms) catalysis: frontiers, opportunities, and challenges. *Journal of Materials Chemistry A*, *7*(8), 3492-3515. https://doi.org/10.1039/C8TA11416A

3. Hammer, B., & Nørskov, J. K. (2000). Theoretical surface science and catalysis - calculations and concepts. *Advances in catalysis*, *45*, 71-129. https://doi.org/10.1016/S0360-0564(02)45013-4

4. Calle-Vallejo, F., Martínez, J. I., & Rossmeisl, J. (2011). Density functional studies of functionalized graphitic materials with late transition metals for oxygen reduction reactions. *Physical Chemistry Chemical Physics*, *13*(34), 15639-15643. https://doi.org/10.1039/C1CP21228A

5. Choi, W. I., Wood, B. C., Schwegler, E., & Ogitsu, T. (2015). Combinatorial Search for high-activity hydrogen catalysts based on transition-metal-embedded graphitic carbons. *Advanced Energy Materials*, *5*(23), 1501423. https://doi.org/10.1002/aenm.201501423

6. Feng, L., Liu, Y., & Zhao, J. (2015). Fe–and Co–P 4-embedded graphenes as electrocatalysts for the oxygen reduction reaction: theoretical insights. *Physical Chemistry Chemical Physics*, *17*(45), 30687-30694. https://doi.org/10.1039/C5CP05551B

7. He, Q., Li, Q., Khene, S., Ren, X., López-Suárez, F. E., Lozano-Castelló, D., ... & Wu, G. (2013). High-loading cobalt oxide coupled with nitrogen-doped graphene for oxygen reduction in anion-exchange-membrane alkaline fuel cells. *The Journal of Physical Chemistry C*, *117*(17), 8697-8707. https://doi.org/10.1021/jp401814f

8. Xu, H., Cheng, D., Cao, D., & Zeng, X. C. (2018). A universal principle for a rational design of single-atom electrocatalysts. *Nature Catalysis*, *1*(5), 339-348. https://doi.org/10.1038/s41929-018-0063-z

9. Zhang, X., Yang, Z., Lu, Z., & Wang, W. (2018). Bifunctional CoNx embedded graphene electrocatalysts for OER and ORR: a theoretical evaluation. *Carbon*, *130*, 112-119. https://doi.org/10.1016/j.carbon.2017.12.121

10. Grimme, S., Antony, J., Ehrlich, S., & Krieg, H. (2010). A consistent and accurate ab initio parametrization of density functional dispersion correction (DFT-D) for the 94 elements H-Pu. *The Journal of chemical physics*, *132*(15), 154104. https://doi.org/10.1063/1.3382344

11. Delley, B. (2000). From molecules to solids with the DMol 3 approach. *The Journal of chemical physics*, *113*(18), 7756-7764. https://doi.org/10.1063/1.1316015

12. Hunter, B. M., Gray, H. B., & Muller, A. M. (2016). Earth-abundant heterogeneous water oxidation catalysts. *Chemical reviews*, *116*(22), 14120-14136. https://doi.org/10.1021/acs.chemrev.6b00398

13. Delley, B. (1990). An all-electron numerical method for solving the local density functional for polyatomic molecules. *The Journal of chemical physics*, *92*(1), 508-517. https://doi.org/10.1063/1.458452

14. Todorova, T., & Delley, B. (2008). Wetting of paracetamol surfaces studied by DMol3-COSMO calculations. *Molecular Simulation*, *34*(10-15), 1013-1017. https://doi.org/10.1080/08927020802235672

15. Zhang, P., Hou, X., Liu, L., Mi, J., & Dong, M. (2015). Two-dimensional π-conjugated metal bis (dithiolene) complex nanosheets as selective catalysts for oxygen reduction reaction. *The Journal of Physical Chemistry C*, *119*(50), 28028-28037. https://doi.org/10.1021/acs.jpcc.5b09148

16. Sha, Y., Yu, T. H., Merinov, B. V., Shirvanian, P., & Goddard III, W. A. (2011). Oxygen hydration mechanism for the oxygen reduction reaction at Pt and Pd fuel cell catalysts. *The Journal of Physical Chemistry Letters*, *2*(6), 572-576. https://doi.org/10.1021/jz101753e

17. Rossmeisl, J., Logadottir, A., & Nørskov, J. K. (2005). Electrolysis of water on (oxidized) metal surfaces. *Chemical physics*, *319*(1-3), 178-184. https://doi.org/10.1016/j.chemphys.2005.05.038

18. Wang, X., Sun, G., Routh, P., Kim, D. H., Huang, W., & Chen, P. (2014). Heteroatom-doped graphene materials: syntheses, properties and applications. *Chemical Society Reviews*, *43*(20), 7067-7098. https://doi.org/10.1039/C4CS00141A

19. Lim, N., Yoo, T. J., Kim, J. T., Pak, Y., Kumaresan, Y., Kim, H., ... & Jung, G. Y. (2018). Tunable graphene doping by modulating the nanopore geometry on a SiO 2/Si substrate. *RSC advances*, *8*(17), 9031-9037. https://doi.org/10.1039/C7RA11601B

Список литературы:

1. Nørskov J. K., Rossmeisl J., Logadottir A., Lindqvist L. R. K. J., Kitchin J. R., Bligaard T., Jonsson H. Origin of the overpotential for oxygen reduction at a fuel-cell cathode // The Journal of Physical Chemistry B. 2004. V. 108. №46. P. 17886-17892. https://doi.org/10.1021/jp047349j

2. Chen Z. W., Chen L. X., Yang C. C., Jiang Q. Atomic (single, double, and triple atoms) catalysis: frontiers, opportunities, and challenges // Journal of Materials Chemistry A. 2019. V. 7. №8. P. 3492-3515. https://doi.org/10.1039/C8TA11416A

3. Hammer B., Nørskov J. K. Theoretical surface science and catalysis - calculations and concepts // Advances in catalysis. 2000. V. 45. P. 71-129. https://doi.org/10.1016/S0360-0564(02)45013-4

4. Calle-Vallejo F., Martínez J. I., Rossmeisl J. Density functional studies of functionalized graphitic materials with late transition metals for oxygen reduction reactions // Physical Chemistry Chemical Physics. 2011. V. 13. №34. P. 15639-15643. https://doi.org/10.1039/C1CP21228A

5. Choi W. I., Wood B. C., Schwegler E., Ogitsu T. Combinatorial Search for high-activity hydrogen catalysts based on transition-metal-embedded graphitic carbons // Advanced Energy Materials. 2015. V. 5. №23. P. 1501423. https://doi.org/10.1002/aenm.201501423

6. Feng L., Liu Y., Zhao J. Fe–and Co–P 4-embedded graphenes as electrocatalysts for the oxygen reduction reaction: theoretical insights // Physical Chemistry Chemical Physics. 2015. V. 17. №45. P. 30687-30694. https://doi.org/10.1039/C5CP05551B

7. He Q., Li Q., Khene S., Ren X., López-Suárez F. E., Lozano-Castelló D., ... Wu G. High-loading cobalt oxide coupled with nitrogen-doped graphene for oxygen reduction in anion-exchange-membrane alkaline fuel cells // The Journal of Physical Chemistry C. 2013. V. 117. №17. P. 8697-8707. https://doi.org/10.1021/jp401814f

8. Xu H., Cheng D., Cao D., Zeng X. C. A universal principle for a rational design of single-atom electrocatalysts // Nature Catalysis. 2018. V. 1. №5. P. 339-348. https://doi.org/10.1038/s41929-018-0063-z

9. Zhang X., Yang Z., Lu Z., Wang W. Bifunctional CoNx embedded graphene electrocatalysts for OER and ORR: a theoretical evaluation // Carbon. 2018. V. 130. P. 112-119. https://doi.org/10.1016/j.carbon.2017.12.121

10. Grimme S., Antony J., Ehrlich S., Krieg H. A consistent and accurate ab initio parametrization of density functional dispersion correction (DFT-D) for the 94 elements H-Pu // The Journal of chemical physics. 2010. V. 132. №15. P. 154104. https://doi.org/10.1063/1.3382344

11. Delley B. From molecules to solids with the DMol 3 approach // The Journal of chemical physics. 2000. V. 113. №18. P. 7756-7764. https://doi.org/10.1063/1.1316015

12. Hunter B. M., Gray H. B., Muller A. M. Earth-abundant heterogeneous water oxidation catalysts // Chemical reviews. 2016. V. 116. №22. P. 14120-14136. https://doi.org/10.1021/acs.chemrev.6b00398

13. Delley B. An all-electron numerical method for solving the local density functional for polyatomic molecules // The Journal of chemical physics. 1990. V. 92. №1. P. 508-517. https://doi.org/10.1063/1.458452

14. Todorova T., Delley B. Wetting of paracetamol surfaces studied by DMol3-COSMO calculations // Molecular Simulation. 2008. V. 34. №10-15. P. 1013-1017. https://doi.org/10.1080/08927020802235672

15. Zhang P., Hou X., Liu L., Mi J., Dong M. Two-dimensional π-conjugated metal bis (dithiolene) complex nanosheets as selective catalysts for oxygen reduction reaction // The Journal of Physical Chemistry C. 2015. V. 119. №50. P. 28028-28037. https://doi.org/10.1021/acs.jpcc.5b09148

16. Sha Y., Yu T. H., Merinov B. V., Shirvanian P., Goddard III W. A. Oxygen hydration mechanism for the oxygen reduction reaction at Pt and Pd fuel cell catalysts // The Journal of Physical Chemistry Letters. 2011. V. 2. №6. P. 572-576. https://doi.org/10.1021/jz101753e

17. Rossmeisl J., Logadottir A., Nørskov J. K. Electrolysis of water on (oxidized) metal surfaces // Chemical physics. 2005. V. 319. №1-3. P. 178-184. https://doi.org/10.1016/j.chemphys.2005.05.038

18. Wang, X., Sun, G., Routh, P., Kim, D. H., Huang, W., & Chen, P. Heteroatom-doped graphene materials: syntheses, properties and applications // Chemical Society Reviews. 2014. V. 43. №20. P. 7067-7098. https://doi.org/10.1039/C4CS00141A

19. Lim N., Yoo T. J., Kim J. T., Pak Y., Kumaresan Y., Kim H., ... Jung G. Y. Tunable graphene doping by modulating the nanopore geometry on a SiO 2/Si substrate // RSC advances. 2018. V. 8. №17. P. 9031-9037. https://doi.org/10.1039/C7RA11601B

Работа поступила
в редакцию 11.01.2021 г.

Принята к публикации
17.01.2021 г.

Ссылка для цитирования:

Chen Fengxiang, Yang Lei The Transition Metal and Non-metal co-Doping Graphene for Oxygen Reduction Reaction Electrocatalysis: a Density Functional Theory Study // Бюллетень науки и практики. 2021. Т. 7. №2. С. 197-207. https://doi.org/10.33619/2414-2948/63/18

Cite as (APA):

Chen, Fengxiang, & Yang, Lei (2021). Transition Metal and Non-metal co-Doping Graphene for Oxygen Reduction Reaction Electrocatalysis: A Density Functional Theory Study. *Bulletin of Science and Practice, 7*(2), 197-207. https://doi.org/10.33619/2414-2948/63/18